International Journal of New Horizons in Physics

http://dx.doi.org/10.18576/ijnhp/030203

Effect of Annealing Temperature on Electrical and Magnetic Properties of $(Nd_{0.6}Sr_{0.4}MnO_3)_{1-x}/(CrO_3)_x$

*A. M. Ahmed, A. K. Diab, H. F. Mohamed and Sara A. Mohamed**

Physics department, Faculty of Science, Sohag University, 82524, Sohag, Egypt.

Received: 21 Feb. 2016, Revised: 28 May 2016, Accepted: 29 May 2016.
Published online: 1 Jul. 2016.

Abstract: The effect of annealing temperature on structural, electrical and magnetic properties of bulk $(Nd_{0.6}Sr_{0.4}MnO_3)_{0.99}/(CrO_3)_{0.01}$ and $(Nd_{0.6}Sr_{0.4}MnO_3)_{0.98}/(CrO_3)_{0.02}$ compositions are investigated. X-ray diffraction show that $(Nd_{0.6}Sr_{0.4}MnO_3)_{1-x}/(CrO_3)_x$(NSMOC) crystallize in a single-phase rhombohedral structure for the as-prepared and annealed samples. Electrical measurement show a metal-semiconductor transition temperature (T_{ms}) for the two compositions. It is observed that T_{ms} increases with thermal treatment. The magnetoresistance MR has a negative sign and it records the highest value for annealed sample at 800ºC for the two compositions. The sign of S is a negative sign for the two compositions. In addition, the calculated Power factor show that the as prepared samples achieve high power factor, therefore our compositions can be considered as the thermoelectric materials.

Keywords: Crystal structure; Electrical properties; Magnetic susceptibility; Seebeck coefficient; Power factor.

1 Introduction

Manganese oxides named as manganites [1,2] have been extensively studied in recent years. Manganites of rare-earth elements are promising materials for today's electronic industry due to established correlation between crystalline structure and "magnetic and transport properties". Many researchers have studied the correlation between ferromagnetism and metallic resistivity in the hole doped region [3-5]. The reasons behind this wide interest in studying manganites, the so-called magnetoresistance MR [6], which is being an important role for a rapid development of new technological such as magnetic sensors based on MR. In addition, the variation of physical properties with the heat treatment which be related the change average particle size and Mn–O bond were a little studying [7-9].

The thermal variant of the electrical resistivity for manganites are identified to be dominated by polaronic transport for $T > T_{ms}$ [10], while below T_{ms}, electron–electron and electron– magnon interactions are usually believed to dominate the conductivity [11-13]. The thermoelectric power (TEP) is an important property to review significant features of the manganites materials [14, 15] including the type of the dominant carrier [16]. Remarkable, in the transition metal oxide, various mechanisms such as diffusion, phonon drag, or magnon drag can influence the TEP [17]. However, deep interpretation of the temperature dependence of Seebeck coefficient (S (T)) is rarely reported [18-20]. The present work aims to study the effect of annealing temperature of $(Nd_{0.6}Sr_{0.4}MnO_3)_{0.99}(CrO_3)_{0.01}$ (NSMOC1) and $(Nd_{0.6}Sr_{0.4}MnO_3)_{0.98}(CrO_3)_{0.02}$ (NSMOC2) on the electrical properties, thermoelectric power and magnetic properties.

2 Experimental

Samples of the two composites (NSMOC1& NSMOC2) were prepared in a required ratio by the conventional solid-state reaction method. The starting chemical Nd_2O_3, $SrCO_3$ and $MnCO_3$ were mixed in stoichiometric proportion to prepare the parent compound $Nd_{0.6}Sr_{0.4}MnO_3$ (NSMO). Nd_2O_3 was dehydrated at 873 K for 6h. The mixture was ground for 6h to ensure homogeneity and presses into pellets under a pressure of 5 ton cm^{-2}. The pellets were calcined twice for 12h at 1173K and then ground at the same conditions. The pellets were ground, mixed and subsequently sintered in air at 1473 K for 30h. The obtained $Nd_{0.6}Sr_{0.4}MnO_3$ (NSMO) powders with single phase perovskite structure, were completely mixed with a high purity CrO_3 powder according to the desired ratio (0.01, 0.02 wt%). The resulting powders $(Nd_{0.6}Sr_{0.4}MnO_3)_{1-x}(CrO_3)_x$ were ground, pelletized at pressure of 5 tons cm^{-2} and then the sintering was repeated at 1273 K for 6h.

The low sintering temperature was chosen to avoid inter-diffusion of NSMO and CrO. Samples were exposed to annealing process for 2 hours at 600, 700, 800 & 900ºC.

The structural characterization was done through X- ray diffraction (XRD) with CuKα radiation at room temperature. The microstructures of samples were studied by Jeol JSM-6610LV scanning electron microscope (SEM). The temperature dependence of resistivity was measured by a standard four-point method at zero field and at 0.6 Tesla in temperature range 80-290K. The ac susceptibility of the composites was measured over the temperature rang 100 to 400K under magnetic field 250 μT and frequency 0.3 kHz using the Barrington Instruments MS2/MS3 Susceptibility/Temperature system. The Curie temperature, T_C is determined by extrapolating the inverse susceptibility $1/\chi$ in the high-temperature range to the temperature axis, via temperature curve. The thermoelectric power measurements were carried out by means of a home-built set-up published in our previous work [12, 21, 22].

3 Results and Discussions

Table 1: Crystal lattice parameters, the cell volume and crystal size of as prepared and annealed NSMOC1 and NSMOC2 samples.

Sample	a(Å)	b(Å)	c(Å)	V(Å^3)	Crystal size(nm)
X=0.010	5.462	7.711632	5.408586	227.8147	16.39
600	5.494	7.718557	5.41517	229.6344	20.40
700	5.424	7.694438	5.422507	226.3063	20.51
800	5.486	7.716808	5.409612	229.0127	19.39
900	5.464	7.702898	5.418748	228.0677	16.4
X=0.020	5.458	7.707111	5.418748	227.9419	15.18
600	5.444	7.702305	5.407597	229.7478	20.00
700	5.474	7.725199	5.409612	228.7603	20.49
800	5.454	7.709931	5.418748	227.8582	20.50
900	5.426	7.693012	5.422507	226.3478	16.37

The X-ray diffraction (XRD) patterns of as prepared and annealed samples of NSMOC1 and NSMOC2 are shown in Fig. 1-a & b. The all patterns can

*Corresponding author e-mail: logien_s@yahoo.com

be indexed by orthorhombic lattice structure. It is observed that the annealing temperature does not affect on the diffraction intensity of the peaks. The lattice parameters, cell volume and crystallite size of samples were calculated and listed in Table (1), where the crystallite size has been estimated using the Scherer formula:

$$\langle CS \rangle = \frac{k\lambda}{\beta \cos(\theta)} \quad (1)$$

Where, k is a constant (k=0.89), λ is a wavelength of X-ray, β is a Full Width Half Maximum (FWHM) of X-ray diffraction peak in radians and θ is a Bragg angle. While the effect of annealing temperature on the lattice parameters, cell volume and crystallite size is small, where it increases or decreases slightly and may be considered almost unchanged. Fig. 2 shows the surface morphology of as prepared and annealed samples at 600ºC for 2 hours of NSMOC1 and NSMOC2. We observe that there is a uniform distribution of grain sizes for the samples. In addition, the grain size increases and porosity decreases with annealing temperature.

The energy dispersive X-ray spectrometer (EDXS) of the as prepared and annealed NSMOC samples are shown in Fig.3. EDXS analysis is used to know the presence of the starting element in the composition. The EDX plot reveals no extra peaks and reflects the presence of all the constituents. All the samples show the exact match for standard peak position for Nd, Sr, Mn, Cr and oxygen (O) in this figure. This reveals that five elemental compositions of all the samples do not contain any foreign element. It is observed from the graph there is no peaks of any impurity and there is no loss of any integrated element after annealing. Fig. 4 shows the variation of resistivity with temperature between 80 and 293K for as prepared and annealed samples of NSMOC1 and NSMOC2. As in Fig. 4 and table 2, all samples achieve a transition at certain temperature

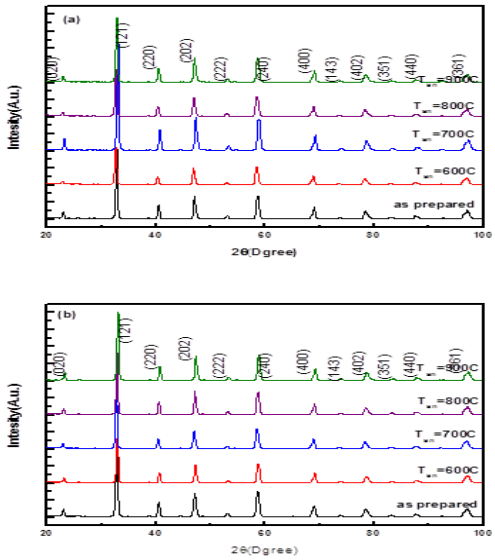

Figure (1): X-ray diffraction patterns of as prepared and annealed samples of a- NSMOC1 and b-NSMOC2 samples.

T_{ms} from metal to semiconductorfor all conditions. For NSMOC1 samples, the resistivity of as prepared and the highest annealing temperature (900 ºC) achieve higher value, this due to the increasing grain boundary where the particle size is smaller as in table 1. As for NSMOC2, the value of resistivity of as prepared is the highest value and then it decreases greater than one order once at first annealing process performed. On the other side, the value of T_{ms} of the two compositions increases once the samples annealed and then it increases slowly (NSMOC1) or it remain stable (NSMOC2). The transition temperature depends on the Mn^{3+} content, which can be altered by different A-site doping or by changing the oxygen stoichiometry [23].

It is well known that the annealing in air may improve oxygen content, modify the grain boundaries and increase particle size of sample. The connectivity between grain boundaries is enhanced by the annealing [24]. In manganites the hopping probability of the e_g electron from Mn^{3+} to Mn^{4+} ion depends on the Mn-O-Mn bond angle [25]. Hence, the decreased in resistivity due to increase Mn^{4+} by annealing process decrease Mn^{3+} ratio, so there is a decrease in distortion that decreases resistivity [11].

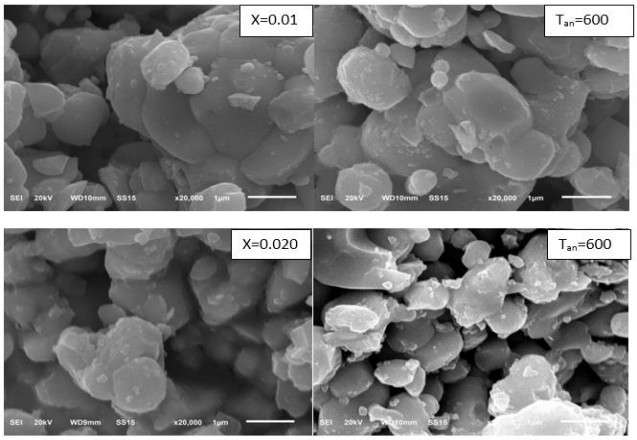

Figure (2): SEM for annealed samples of a- NSMOC1 and b-NSMOC2 samples

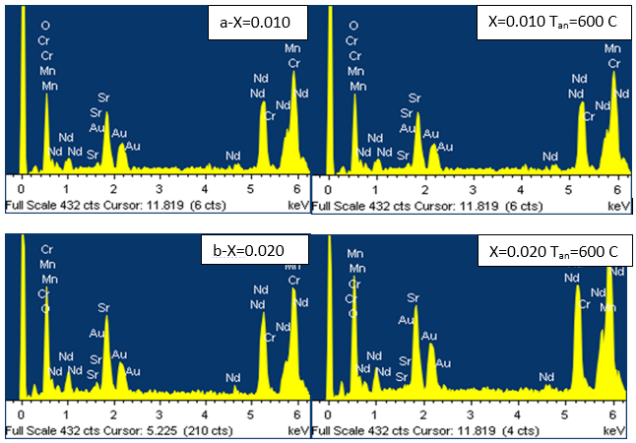

Figure (3): EDXS of as prepared and annealed samples of a- NSMOC1 and b-NSMOC2 samples.

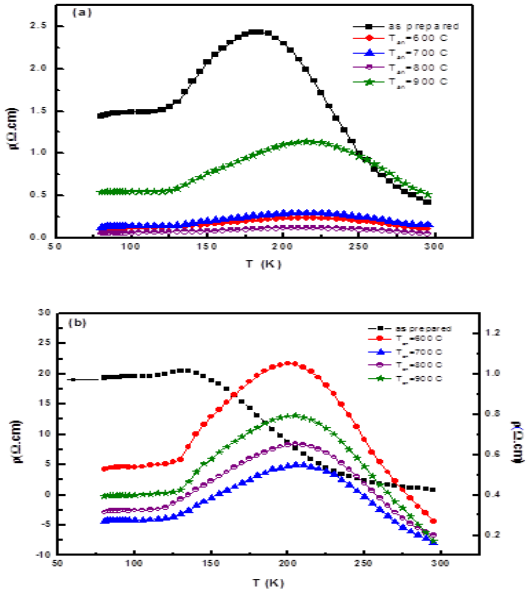

Figure (4) The temperature dependence of the resistivity of a- NSMOC1 and b-NSMOC2 samples.

Table 2: $T_{ms,}$ MR% and $\rho_{0,}$ ρ_2 &$\rho_{4.5}$ values of NSMOC composite.

Sample	T_{an} (^{0}C)	T_{ms} (K)	MR% around T_{ms}	MR%(room temperature	ρ_o (Ω.cm)	ρ_2*10^{-5} (Ω.cm/ K^2)	$\rho_{4.5}$* 10^{-11} (Ω.cm /K4.5)
0.010	as-prepared	185	3.6	1.8	1.31	1.22	-6.22
	600	215	4.5	1.53	0.084	0.288	0.12
	700	220	9.5	1.5	0.092	0.453	0.038
	800	215	9	2.8	0.036	0.195	-.0173
	900	215	2.5	0.8	0.42	1.22	0.848
0.020	as-prepared	130	14.7	5.2	-11.4	-11.4	76.7
	600	200	-2.67	-3.6	1.12	1.12	1.3
	700	205	10.2	2.5	0.53	0.53	0.62
	800	205	27.1	38.3	0.87	0.87	0.42
	900	205	9.5	5.9	0.94	0.94	0.71

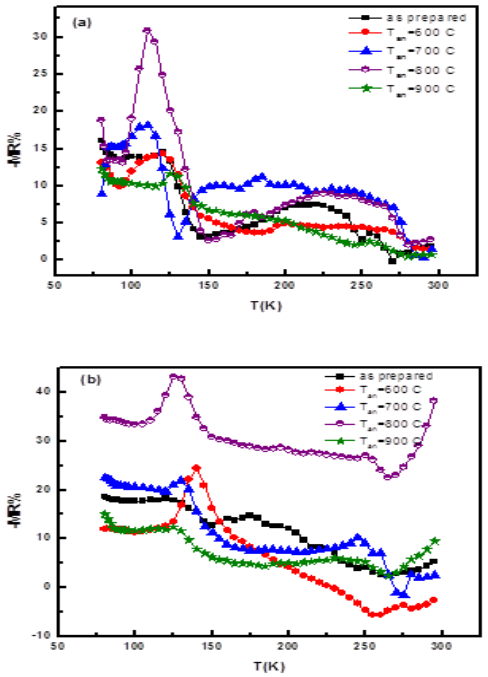

Figure (5): Magnetoresistance vs. temperature as a function of annealing temperature of a- NSMOC1 and b-NSMOC2 samples.

Applied magnetic field causes a decrease in resistivity throughout the temperature range and it shifts T_{ms} a little to higher temperature [21, 22, 26]. This shift is due to alignment of the Mn spins that causes the suppression of the semiconducting state by metallic state. Because of the spin ordering, the charge carries also suffer less scattering with increase of the exchange interaction, hence the resistivity decreases and a large negative magnetoresistance occurs.The value of magnetoresistance can be calculated as:

$$MR = \frac{\rho(H)-\rho(0)}{\rho(0)}\% \qquad (2)$$

Where $\rho(H)$ and $\rho(0)$ are the resistivity with and without magnetic field, respectively.

Fig. 5 shows the plots of magnetoresistance (MR) as function of temperature for as prepared and annealed samples of NSMOC. In general, all samples have a peak nearly the transition temperature; see Fig. 5 and table 2. So as to analyze the temperature dependence of MR% plots sketched in Fig. 5, there are two different mechanisms describe the appeared maximum magnetoresistance should be taken in consideration.

The first one is the intrinsic magnetoresistance (iMR) which arises due to

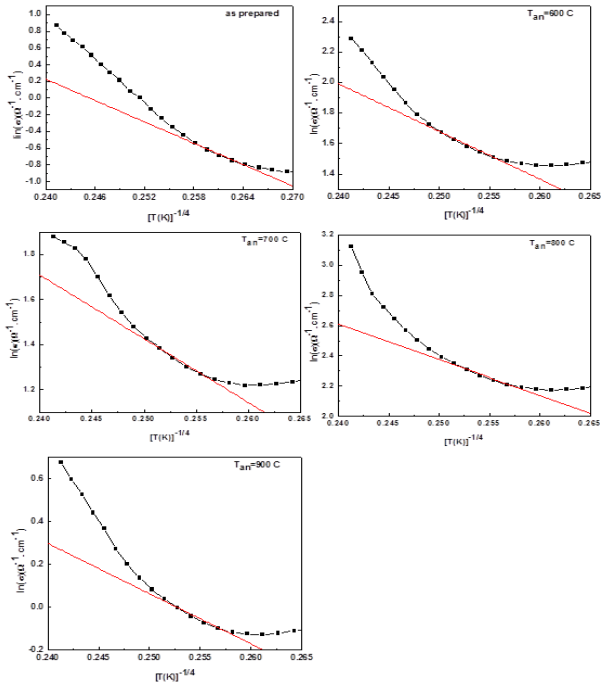

Figure (6 a): ln(σ) versus $(T)^{-1/4}$ for as preparedand annealing samples of NSMOC1, the solid line indicates the best fit to the (VRH) model between T_{ms} and $\theta_D/2$.

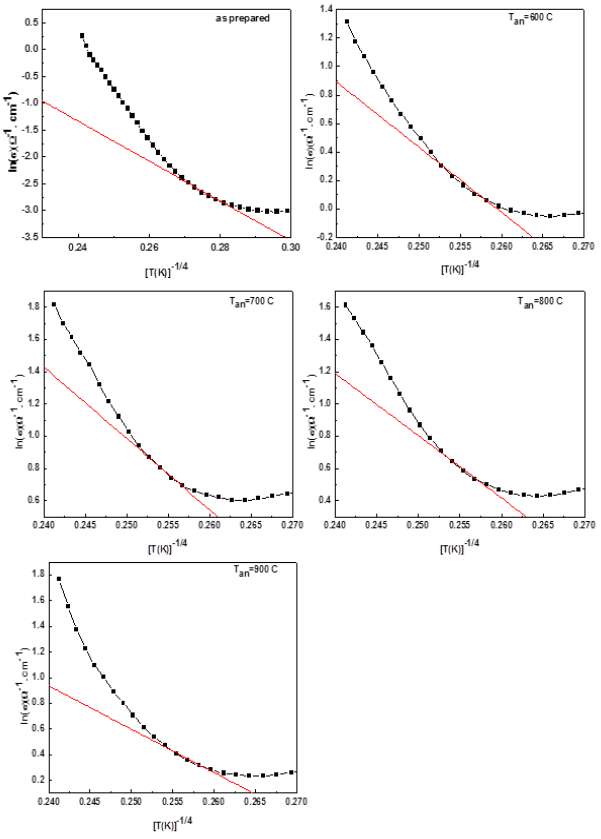

Figure (6 b): ln(σ) versus $(T)^{-1/4}$ for as preparedand annealing samples of NSMOC2 the solid line indicates the best fit to the (VRH) model between $T_{ms}$and $\theta_D/2$.

the suppression of spin fluctuations by aligning the spins due to applying of the magnetic field. Note that, the maximum of the iMR near the ferromagnetic transition temperature. The second one is the extrinsic magnetoresistance (eMR) which arises due to inter-grain spin polarized tunneling across the grain boundaries [8, 27, 28]. Appearance of the two maxima in the MR-T plots (see Fig.6), confirm that both mechanisms are strongly effective in the present case. At low temperature ($T<T_{ms}$), the conduction mechanism in the ferromagnetic metallic region can explain by fitting ρ(T) data was found to be well represented by the empirical relation (as seen in Fig. 6)

$$\rho = \rho_o + \rho_2 T^2 + \rho_{4.5} T^{4.5} \quad (3)$$

where the terms ρ_0 [29], $\rho_2 T^2$ and $\rho_{4.5} T^{4.5}$ are arise due to the grain/ domain boundary, the electron-electron scattering and the electron-magnon scattering process which may be likely to arise due to spin-wave scattering process respectively. The well-fitting indicate that the resistivity is due to electron-electron scattering and electron-magnon scattering beside the resistivity that due to grain boundaries. The decreasing in the resistivity with increasing the annealing temperature well agreement with the increasing in the grain size (decreasing the grain boundaries) see table 1. The change in ρ_2 and $\rho_{4.5}$ is an un- sequential and independent on the annealing temperature (see table 2).

The resistivity's data above T_{ms} (PM–S region) are divided into two distinct parts,one is Mott's variable range hopping (VRH) at $\theta_D/2 \geq T \geq T_{ms}$ and the second is small polaron hopping (SPH) at $T>\theta_D/2$.

With respect to the VRH model that has the formula [30]

$$\sigma = \sigma_o \exp\left(\frac{T_o}{T}\right)^{\frac{-1}{4}} \quad (4)$$

Where T_0 is the Mott characteristic temperature and expressed as the density of states in the vicinity of Fermi energy, $N(E_F)$ and localization length "1/a" as follows:

$$T_o = \frac{18a^3}{k_B N(E_F)} \quad (5)$$

Where a=2.22 nm^{-1} has been reported by Virt *et al.* [31].

The experimental data of the VRH models are shown in Fig.6 for as prepared and annealed samples of NSMOC. As evident in table 3&4, the value of T_0 decreases with increasing the annealing temperature $T_{an}$for the two compositions. This due to the increasing in the density of state with increasing T_{an}. The value of $\theta_D/2$ greater than T_{ms}, this indicate that the range of VRH is a wide range. In addition, θ_D shifts to high temperature after the thermal treatment of NSMOC1, this indicate the expansionof VRH range with increasing the annealing temperature. In the semiconductor range at $T > \theta_D/2$ the conduction takes place by the hopping of small polarons, but they hop only to the nearest neighbors and are assisted by the thermal energy, then the conduction data dominated by the thermally activated hopping of small polarons. The data have fitted to the SPH model [29,32,33] which gives:

$$\frac{\rho}{T} = \rho_\alpha \exp\left(\frac{E_\rho}{k_B T}\right) \quad (6)$$

Where, ρ_α is the resistivity coefficient and is given by:

$$\rho_\alpha = \left[\frac{k_B}{\upsilon_{ph} N e^2 R^2 C(1-C) \exp(2\alpha R)}\right] \quad (7)$$

k_B is the Boltzman constant and T is the temperature (kelvin), N is the number of ions site per unit volume, $R \approx (1/N)^{1/3}$ is the average interests spacing, C is the fraction of sites occupied by polaron, α is the electron wave function decay constant, ν_{ph} is the optical phonon frequency. For NSMOC1, the value of υ_{ph} ($h\nu_{ph}=k_B\theta_D$) of as prepared sample less than the value of υ_{ph} of annealed samples this indicate that the frequency of lattice wave increase after the thermal treatment. With respect of NSMOC2, the frequency of lattice wave decreasesonce annealing at 600 °C then it is constant. The values of υ_{ph}, θ_D and T_{ms} have the same behavior for all samples.

The relation between ρ/T and 1/T plotted in Fig. 6 for as prepared and annealed samples of NSMOC. In addition, all parameters as eq. (6) - (9) were calculated and listed in table 3&4. As in table 3(NSMOC1) the value of E_ρ after annealing less than E_ρ of the as prepared samples. The value of E_ρ is inversely proportional to the grain sizes, which mean that with increasing grain size lead to increase the connectivity between grains moreover, increases cooperation of the conduction electrons to hop the neighboring size [35]. The decreasing in E_ρ with thermal treatment can be explained by the core-shell model proposed by [36]. The change of value of E_ρ of NSMOC2 like N shape. The increasing in E_ρ due to the oxygen deficiency might be responsible for bending of Mn-O-Mn bond angle, which in turn might make the bandwidth narrower enhancing the effective mass of the charge carrier. Due to this, the effective band gap increases with increasing oxygen deficiency. Therefore, higher values of activation energies needed for the charge carriers to overcome this band gap are justified [37,38].

Table (3): T_c, T_N, E_ρ, hoping parameters as function of annealing temperature of NSMOC1.

Sample	As prepared	600	700	800	900
T_C (K)	276	275	272	269	269
T_N(K)	128	112	120	115	118
θ_D(K)	459.7	500	500	526.3	500
ν_{ph}(Hz)x10^12	9.5	10.4	10.4	10.9	10.4
ρ_ox10^-6	4.4	1.8	6.2	0.7	21.2
E_ρ(meV)	146.7	132.6	110.5	138.9	84.4
W_H(meV)	99.8	85.7	63.6	92.05	37.5
$W_{H/3}$(meV)	33.2	28.5	21.2	30.6	12.5
W_D(meV)	199.7	171.4	127.3	184.10	75.02
H(mev)	27.7	27.8	25.8	29.1	22.6
J(meV)	23.6	25.1	25.1	26.1	25.1
σ_ox10^3(mΩcm)$^{-1}$	0.004	0.013	0.005	0.004	0.000
ρ_ox10^3(Ωcm)	259.2	75.1	201.6	254.2	2685.2
T_o(K)x10^6	1.3	0.9	0.6	0.31	0.30
N(E_F)(eV-1 cm^{-3})x10^20	14.8	21.3	31.5	65.3	67.4
Nx10^23	27.1	38.8	57.4	119.1	122.8
R(À)x10^-7	1.4	1.3	1.19	0.99	0.98
W(meV)	53.3	48.7	44.2	36.8	36.5
αR	3.2	2.9	2.6	2.2	2.1
T_S(K)	195.5	205.5	225.5	225.5	215.5

The activation energy [34] is given by eq.

$$E_\rho = W_H + \frac{W_D}{2} \text{for } (T>\theta_D/2) \quad (8)$$

$$E_\rho = W_D \quad \text{for } (T<\theta_D/4) \quad (9)$$

Where W_H is the polaron hopping energy and W_D is the disorder energy.

In order to study the effect of annealing on polaronic transport, the ρ(T) data was fitted to both the adiabaticas well as non-adiabatic polaron hopping models of E_{min} and Holstein.

Adiabatic polaron hopping: In this case the relevant optical mode lattice fluctuationislong lived compared to the electron tunneling event J>H. Non-adiabatic polaron hopping: In the non-adiabatic limit the electron tunneling event is not necessarily fast compared to the relevant optical-mode lattice fluctuation J<H.As seen in table 3&4, all samples of NSMOC1 and NSMOC2have a non adiabatic conduction since J<H except at T_{an}=900°C of NSMOC1 has an adiabatic conduction

The magnetic susceptibilityis shown in Fig.7 for the as prepared and annealed samples of the two composites.

All samples achieve Ferro- paramagnetic transition at a certain temperature, Curie temperature (T_C). Moreover,the samples show antiferromagnetic phase at low temperature at certain temperature Neel temperature (T_N)

depend on the content of CrO_3 and the temperature of annealing as in tables 3 &4. The Neel temperature values are ranging from 112 to 128 K of NSMOC1 and 126 to 173 of NSMOC2 as in tables 3& 4, this was confirmed in magnetization measurements [39].

Table (4): T_c, T_N , E_ρ, hoping parameters as function of annealing temperature of NSMOC2.

Sample	As prepared	600	700	800	900
T_C (K)	275	288	273	269	272
T_N (K)	127	173	137	126	138
θ_D(K)	510.2	487.8	487.8	487.8	487.8
ν_{ph}(Hz)x10^12	10.6	10.1	10.1	10.1	10.1
ρox10^-6	1.04	2.6	1.7	2.4	0.5
E_ρ(meV)	141.8	149.8	146.9	142.8	178.3
W_H(meV)	94.9	102.9	100.09	95.9	131.4
$W_{H/3}$(meV)	31.6	34.3	33.3	31.9	43.8
W_D(meV)	189.9	205.9	200.1	191.8	262.9
H(mev)	28.9	28.8	28.6	28.3	30.6
J(meV)	25.5	24.7	24.7	24.7	24.7
σ_ox10^3(mΩcm)^-1	8139.5	0.14	0.17	0.035	0.009
ρ_ox10^3(Ωcm)	0.000	6.9	5.8	28.6	117.3
T_o(K)x10^6	78.7	4.3	3.8	2.2	1.3
N(EF)(eV-1 cm-3)x10^20	0.25	4.6	5.2	9.1	15.5
Nx10^23	0.4	8.4	9.6	16.6	28.3
R(À)x10^-7	3.9	1.9	1.8	1.6	1.4
W(meV)	147.08	71.4	69.09	60.3	52.8
αR	8.8	4.2	4.1	3.6	3.1
T_S(K)	185.5	195.5	195.5	205.5	205.5

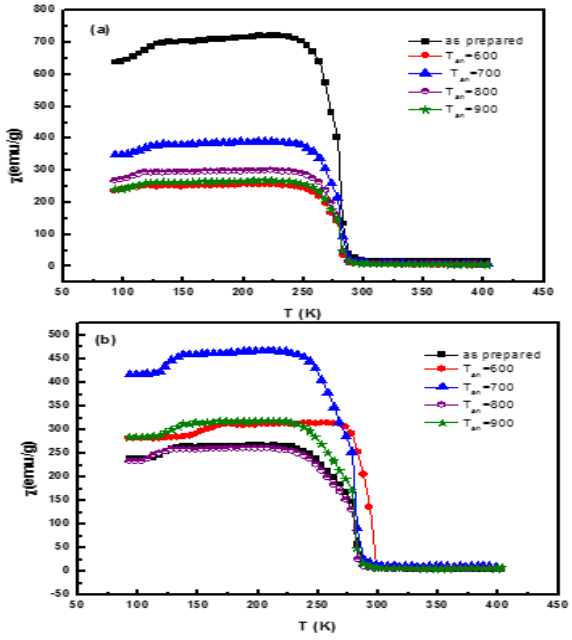

Figure (7): Temperature dependence of susceptibility for annealed samples of a- NSMOC1 and b-NSMOC2 samples.

On the other side, the value of χ change un-symmetry with annealing temperature. For NSMOC1 the highest and lowest value belong to as prepared and first annealing temperature respectively. For the higher doping NSMOC2, it is observed that the broad of phase transition indicates an inhomogeneous magnetic state, which can be due to a high concentration of defects and their inhomogeneous distribution. On the other hand, the values of T_C are convergent, and the small change is un-sequentially (see tables 3&4).

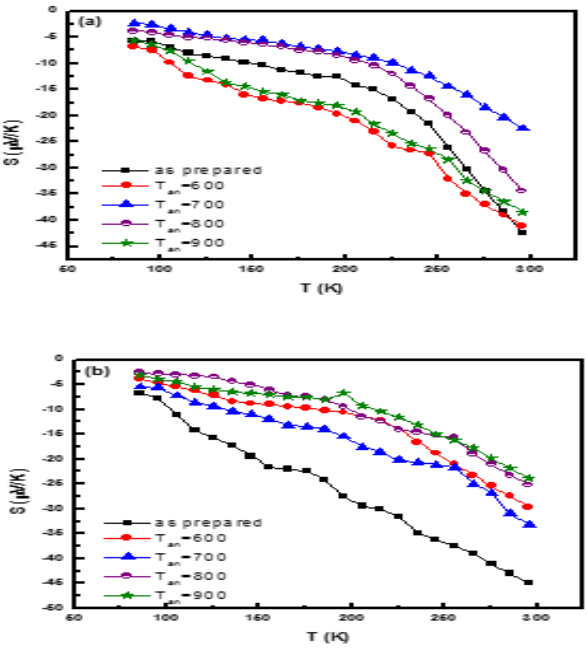

Figure (8): S versus T for a- NSMOC1 and b-NSMOC2 samples for 2h at different annealing temperature.

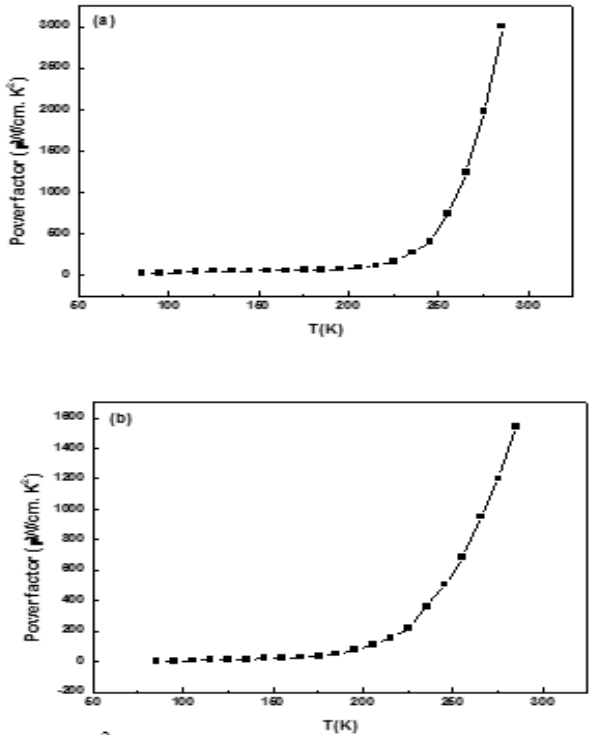

Figure (9): The power factor S^2/ρ plotted as a function of the temperature of as prepared a- NSMOC1 and b-NSMOC2 samples.

Fig. 8 show the dependence of Seebeck coefficient on the temperature of as prepared and annealed samples of the two composites. The thermoelectric power of these samples is a negative sign over a temperature range, the values of S are in Microvolt range and all samples have a one peak represent the transition temperature from thermopower data (T_s) due to metal insulator transition[40]. The transition temperatures (T_s) have a shift to high temperature range with increasing the annealing temperature for the two compositions. T_s express the T that the slope of S(1/T) change. As in figures, the negative value of S increases with increasing temperature for the as prepared and annealed samples of the two composites. The change of value of S with T_{an} change un-sequentially. A somewhat, it is observed that the values of T_s are approaching in values and behavior of the T_{ms} values of the two composites, which indicates there are a correlation between electrical and thermoelectric properties.

The combination between S and ρ factors makes them good candidates to know if this material is a thermo- generationapplications, with calculate the power factor (P):

$$P = \frac{S^2}{\rho} \quad (10)$$

Fig. 9show the power factor versus T for as prepared samples, which has been calculated from ρ and S. It is observed that the values ofP increase with increasing the ambient temperature. The increasing of value speed at high temperature range (T>200C). It is observed that the value of Pis in micro, which can considered that it is a high value of power factor compare with other semiconductor materials. The conclusion of our results is two samples have high value of P due to the high value of S.

4 Conclusion

Structure, electrical and magnetic properties have been studied ofNSMOC1 and NSMOC2 for as prepared and annealed samples. All samples have a single-phase orthorhombic structure. The resistivity decrease with increasing the annealing temperature. The value of calculated magnetoresistance (MR) shows a peak nearly the Metal- Semiconducting transition temperature. Annealed sample at 800ºC for the two composites achieved the highest value of magnetoresistance. Susceptibility measurements show that all samples have Ferro-paramagnetic transition at Curie temperature and antiferro-ferromagnetic at low temperature at Neel temperature. The Seebeck coefficient (S) values have a negative sign over temperature range.

It is observed that there are a correlation between electrical and thermoelectric power from the values of T_s and T_{ms}. The value of the power factor show that the two composites have a high value of power factor.

References

[1] E. D. Wollan and W. C. Koehler, Physical Review Letters**100**, 545, 167-168 (1955).

[2] J. B. Goodenough, Physical Review letters **100**, 564-573 (1955).

[3] G.H. Jonker and J.H. van Santem, Physica **16**, 337-349 (1950).

[4] C. Zener, Physical Review letters **81**, 440-443(1951).

[5] C. Zener, Physical Review letters **82**, 403- 405 (1951).

[6] 6-R.yon Helmot, J. Wecker, B. Holzapfel, L. Schultz, K. Samwor, Physical Review letters**71**, 2331-2333 (1993).

[7] 7-E. Dagotto, T. Hotta, and A. Moreo, Physics Reports **344**,1-153 (2001).

[8] 8-A.-M. Haghiri-Gosnet and J.-P.Renard, Journal of Physics D **36**, R127-R150(2003).

[9] 9-Y. Tokura and Y. Tomioka, Journal of Magnetism and Magnetic Materials **200**,1-23 (1999).

[10] 10-P.G. Collins, K. Bradley, M. Ishugami, and A. Zettl, Science **287**, 1801-1804 (2000).

[11] 11-A. M. Ahmed, S. A. Saleh, E.M.M. Ibrahim, E. Bontempib, , H. F. Mohamed,Journal of Magnetism and Magnetic Materials **320** , L43-L49 (2008).

[12] 12-A.M. Ahmed, Physica B **352**, 330-336 (2004).

[13] 13-A. M. Ahmed, H. F. Mohamed, A. K.Diab, Abd El-Mo'ez A Mohamed, A. E. A.Mazen, Aml M. Mohamed, Indian Journal Physics **89(6)**, 561-570 (2015).

[14] 14-F. J. Baltt, P. A. Schoreder, C. L. Foiles, and D. Gerig, Thermoelectric power of metals (Plenum, New York)(1976).

[15] 15-A.M. Ahmed, S. A. Saleh, E. M. M. Ibrahim, H.F. Mohamed, Journal of Magnetism and Magnetic Materials **301**, 452-457 (2006).

[16] 16- P. G. Collins, K. Bradley, M. Ishugami and A. Zettl, Science. 287, 1801 (2000).

[17] 17- E.S. Choi, J. S. Brooks, J.S. Qualls, and Y.S. Song, Review of Scientific Instruments**72**, 2392-2397 (2001).

[18] 18-W,-H. Jung, Journal of Korean Ceramic Society **40**, 849-854 (2003).

[19] 19-P. Mandal, Physical Review B **61**, 14675-14678 (2000).

[20] 20-S. Bhattacharya, A. Banerjee, S. Pal, R. K. Mukherjee, and B. K. chaudhuri, Journal of Applied Physics **93**, 356-361 (2003).

[21] 21- A. M. Ahmed, G. Papavassiliou , H. F. Mohamed, E. M. M. Ibrahim, Journal of Magnetism and Magnetic Materials **392**, 27–41 (2015).

[22] 22- A. M. Ahmed, M. R. Ahmed, S. A. Ahmed, Journal Electromagnetic Analysis &Applications **3**, 27-32 (2011).

[23] 23-H. L. Ju, J. Gopalakrishnan, J. L. Peng, Qi Li, G. C. Xiong, T. Venkatesan, and R. L. Greene

[24] Physical Review B **51**, 6143(R)-6146(R) (1995).

[25] 24- H. L. Ju, H.C. Sohn and Kannan M. Krishnan, Physical Review Letters**79**, 3230-3233 (1997)

[26] 25- D. C. Worledge, G. J. Snyder, M. R. Beasley, T. H. Geballe, R. Hiskes, S. DiCarolis, *Journal* of Applied Physics **80**, 5158-5161 (1996).

[27] 26- A. M. Ahmed, M. A. Abedellateef, H. A. Abd El-Ghanny, and Abd El Moez A. Mohamed, Phys. Status Solidi A **212**, No. 3, 623–631 (2015).

[28] 27- A. Gupta, G. Q. Gang, G. Xiao, P. R. Duncombe, P. Lecoeur, P.Trouilloud, Y. Y.Wang, V. P. Dravid, J. Z. Sun, Physical Review B **54**, R15629(R)-R15633(R) (1996).

[29] 28- H.Y.Hwang, S. W.Cheong, N. P. Ong, B. Batlogg, Physical Review Letters **77**, 2041-2044 (1996).

[30] 29-M. Batlabyal, A. Ray, T. K. Deytc, Indian Journal of pure & Applied Physics **41**, 443-447 (2003).

[31] 30- N. F. Mott and E. A. Davis, 2nd edn. (Clarendon Press,Oxford, 2012).

[32] 31- M. Viret, L. Ranno, J. M. D. Coey, Physical Review B **55**, 8067-8070 (1997).

[33] 32-G. Jeffrey Snyder, R. Hiskes, S. Dicarolis, M. R. Beasley, and T. H. Geballe, Physical Review B **53**, 14434-14444 (1996).

[34] 33-A. Banerjee, S. Pal and B. K. Chaudhuri, Journal of Chemical Physics **115**,1550-1558(2001).

[35] 34-I. G. Austin and N. F. Mott, Advances in Physics **18**, 41-102 (1969).

[36] 35-G. Venkataiah, D. C. Krishna, M. Vithal, S. S. Raw, S. S. Bhat, V. Prasad, S. V. Subramanyam, P. Venugopal Reddy, Physica B **357**, 370-379 (2005).

[37] 36-N. Zhang, W. Ding, W.Zhong, D. Xing and Y. Du, Physical Review B **56**, 8138-8142 (1997).

[38] 37-L. Malavasi, M. C. Mozzati, C. B. Azzoni, G. Chiodelli, G. Flor, Solid State Communications **123**, 321-326 (2002).

[39] 38- S. Bhattacharya, R. K. Mukherjee, B. K. Chaudhuri, Applied Physics Letters, **82**, 4101-4103(2003).

[40] 39- M. Hehnion, F. Moussa, G. Giotteau, J. Rodriguez-Carvajal, L. Pinsard, and A. Revcolevschi, Physical Review Letters **81**, 1957-1960 (1998).

[41] 40- S. Bhattacharya, R. K. Mukherjee, and B. K. Chaudhuri, Applied physics letters **82**, 4101-4103 (2003).